Journal of Molecular Cell Biology (2022), 14(3), mjac014 https://doi.org/10.1093/jmcb/mjac014
Published online March 8, 2022

Article

Incorporation of a histone mutant with H3K56 site substitution perturbs the replication machinery in mouse embryonic stem cells

Xuan Kang [1,*], Xiaomei Yang[1], Xiaobo Guo[1], Yabin Li[1], Chenxin Yang[1], Huimin Wei[1,2,*], and Jianfeng Chang[1,*]

[1] Research Center for Translational Medicine, East Hospital, School of Life Sciences and Technology, Tongji University, Shanghai 200092, China
[2] Tsingdao Advanced Research Institute, Tongji University, Qingdao 266071, China
* Correspondence to: Xuan Kang, E-mail: 2011kangxuan@tongji.edu.cn; Huimin Wei, E-mail: hmwei@tongji.edu.cn; Jianfeng Chang, E-mail: jfchang@tongji.edu.cn

Edited by Zhiyuan Shen

Sense mutations in several conserved modifiable sites of histone H3 have been found to be strongly correlated with multiple tissue-specific clinical cancers. These clinical site mutants acquire a distinctively new epigenetic role and mediate cancer evolution. In this study, we mimicked histone H3 at the 56th lysine (H3K56) mutant incorporation in mouse embryonic stem cells (mESCs) by lentivirus-mediated ectopic expression and analyzed the effects on replication and epigenetic regulation. The data show that two types of H3K56 mutants, namely H3 lysine 56-to-methionine (H3K56M) and H3 lysine 56-to-alanine (H3K56A), promote replication by recruiting more minichromosome maintenance complex component 3 and checkpoint kinase 1 onto chromatin compared with wild-type histone H3 and other site substitution mutants. Under this condition, the frequency of genomic copy number gain in H3K56M and H3K56A cells globally increases, especially in the *Mycl1* region, a known molecular marker frequently occurring in multiple malignant cancers. Additionally, we found the disruption of H3K56 acetylation distribution in the copy-gain regions, which indicates a probable epigenetic mechanism of H3K56M and H3K56A. We then identified that H3K56M and H3K56A can trigger a potential adaptation to transcription; genes involved in the mitogen-activated protein kinase pathway are partially upregulated, whereas genes associated with intrinsic apoptotic function show obvious downregulation. The final outcome of ectopic H3K56M and H3K56A incorporation in mESCs is an enhanced ability to form carcinomas. This work indicates that H3K56 site conservation and proper modification play important roles in harmonizing the function of the replication machinery in mESCs.

Keywords: H3K56A/M mutants, replication promotion, replication stress, transcriptional adaptation, mouse embryonic stem cells

Introduction

Core histone H3, one of the four highly conserved chromatin scaffold proteins, can be extensively modified; this process involves important pathways of epigenetic regulation. Although the identical amino acid sequence of H3 is highly conserved, *de novo* single-nucleotide substitution occurs on the coding sequence of H3.1 clusters or H3.3 alleles, producing novel sense mutants in which the variant sites function as driver mutations in clinical tumor cases (Wan et al., 2018). In next-generation high-throughput screens, sense mutations of coding genes, including *HIST1H3B*, *H3F3A*, and *H3F3B*, were found to produce a series of histone mutants in multiple clinical cases and were considered tumor driver mutations. It has been reported that 78% of pediatric diffuse intrinsic pontine gliomas (DIPGs) and 22% of non-brainstem pediatric glioblastomas (non-BS-PGs) exhibit a mutation in *H3F3A* or in *HIST1H3B* caused by a p.Lys27Met (p.K27M) substitution (Wu et al., 2012). An additional somatic mutation in *H3F3A* with p.Gly34Arg alteration was also detected in non-BS-PGs. Moreover, 95% of chondroblastomas contained a p.K36M alteration in *H3F3B*, whereas 92% of giant cell tumors of bone carried p.Gly34Trp or p.Gly34Leu alterations exclusively in *H3F3A* (Behjati et al., 2013).

Received July 23, 2021. Revised February 23, 2022. Accepted March 4, 2022.

The mechanism underlying the effect of histone driver mutants is associated with their dominance in re-establishing the whole epigenetic landscape, and incorporation of histone mutants disrupts faithful epigenetic inheritance and facilitates the adaptation and evolution of malignant cells (Lewis et al., 2013; Fang et al., 2016; Lu et al., 2016). The reported clinical K>M alterations at conserved positions in H3 can specifically inhibit the activity of site-specific SET-motif-containing methyltransferase in a conserved binding–killing mechanism (Lewis et al., 2013).

In addition to the highly frequent driver mutations, a large number of rare or low-frequency histone H3 sense mutations were also found and collected in the carcinoma database Catalogue of Somatic Mutations in Cancer (COSMIC). However, whether these mutations are associated with the pathogenic process of cancers or occur without clinical importance is still unknown. All these sense mutations involve some important modifiable sites, including the 56th amino acid (lysine, K) of histone H3 (H3K56), which is located within the globular domain and near the DNA entry and exit sites on the nucleosome and can be modified by adding acetyl or methyl groups (mono- and tri-) to its ε-amino group (Masumoto et al., 2005; Yu et al., 2012). H3K56 acetylation (H3K56ac) has been frequently studied and reported to play important roles in multiple processes, including transcription, replication, and DNA damage repair in yeast (Xu et al., 2005; Han et al., 2007; Chen et al., 2008; Li et al., 2008; Williams et al., 2008). K56 of the newly synthesized H3 is fully acetylated and deposited on chromatin in a replication-dependent manner, and the specific acetyltransferase Rtt109 and histone chaperone anti-silencing factor 1 (Asf1) contribute to this process in yeast (Recht et al., 2006; Han et al., 2007). H3K56ac is less abundant in mammals than in yeast, and there is controversy regarding its replication coupling function, but H3K56 monomethylation (H3K56me1) seems to be able to compensate for this effect by supplying a docking site for the activation of proliferating cell nuclear antigen (PCNA) (Corpet and Almouzni, 2009; Yu et al., 2012). In *Saccharomyces cerevisiae*, H3K56ac finely regulates the activity of DNA synthesis coupled with DNA breakage repair, which limits extensive repair synthesis and thus prevents genome instability (Chen et al., 2008; Che et al., 2015). In mammals, accumulating evidence indicates a similar importance of H3K56ac in maintaining replication fidelity and genome integrity (Das et al., 2009). However, these findings indicate additional challenges because of the drawbacks of commercial antibodies (Corpet and Almouzni, 2009; Pal et al., 2016). In addition, the importance and clinical outcome of H3K56 site mutation, especially H3 lysine 56-to-methionine (H3K56M) searched in the cancer database, still remain unclear.

Previous research has suggested that site substitution can mimic the change in charge caused by histone modification (Masumoto et al., 2005). Furthermore, artificial histone site-specific mutants are also used to define the mechanism of the related modifications and histone code (Dai et al., 2008; Shan et al., 2016). In this study, we adopted the H3K56M mutant, a histone mutant found in carcinomas, and other types of mutations, including H3 lysine 56-to-alanine/glutamine/arginine (H3K56A/Q/R), to analyze cellular adaptation in mouse embryonic stem cells (mESCs). We found that H3K56 site substitution directly disrupted the balance of replication in mESCs. H3K56M and H3K56A mutants specifically exhibited higher affinity for both checkpoint kinase 1 (Chk1) and minichromosome maintenance complex component 3 (MCM3), which finally facilitated the origin recognition complex (ORC) to function smoothly on the host chromatin template. All these pieces of evidence will allow us to further understand the importance of H3K56 conservation and modification.

Results

Incorporation of H3K56 site substitution mutants in mESCs interferes with DNA replication

By scanning for K>M mutations in the COSMIC database, we found p.K57M (the 56th residue of mature protein) somatic substitution on *HIST1H3E* in addition to p.K36M and p.K27M in other alleles of histone H3.1 or H3.3 (Figure 1A). To study the potential of histone H3K56M in cellular processes, we primarily constructed a series of histone H3K56 site mutants and incorporated them into mESCs by lentivirus-mediated ectopic expression (Supplementary Figure S1A–C). We also constructed other cell lines carrying the H3K56 mutants fused with enhanced green fluorescent protein (EGFP) and evaluated the ratio of exogenous H3 to endogenous H3 by immunoblotting. The data showed that H3K56 mutants were ∼5% of total H3 histones (Supplementary Figure S1D). We selected H3K56A as a mimic of depolarization of a single site, such as H3K56M, by depleting the modification of the docking site on the side chain. Furthermore, we adopted H3K56Q as a mimic of charge elimination, such as H3K56ac, and H3K56R as a side chain similarity mimic of H3K56. After multiple rounds of fluorescence-assisted cell sorting (FACS) purification from single cells, we obtained stable strains of mESCs carrying H3K56 mutants, and the clonal morphology and pluripotency with strong alkaline phosphatase staining showed no obvious change compared with the wild-type H3-carrying strain (H3WT) (Supplementary Figure S1B). Then, we tested the replication efficiency by detecting EdU labelling intensity using FACS analysis and confocal imaging (Figure 1; Supplementary Figure S2). The relative intensity of EdU labelling in both H3K56M and H3K56A strains showed an obvious increase compared with H3WT (Figure 1B and C). H3K56M and H3K56A strains also showed enhanced EdU incorporation and increased mean EdU incorporation in S phase compared with H3WT (Figure 1D and E). However, the H3K56Q mutant strain showed a decrease compared with H3WT, and the H3K56R strain did not show obvious change (Figure 1F–I; Supplementary Figure S2). All these data indicated that a type-specific H3K56 site substitution, especially H3K56M and H3K56A, could obviously perturb the replication process in mESCs. We further found that the proportion of H3K56M and H3K56A cells in S phase was actually lower than that of H3WT cells, as determined by propidium iodide staining, while the proportion of H3K56M and H3K56A cells in G2/M phase increased slightly (Supplementary Figure S3). Overall,

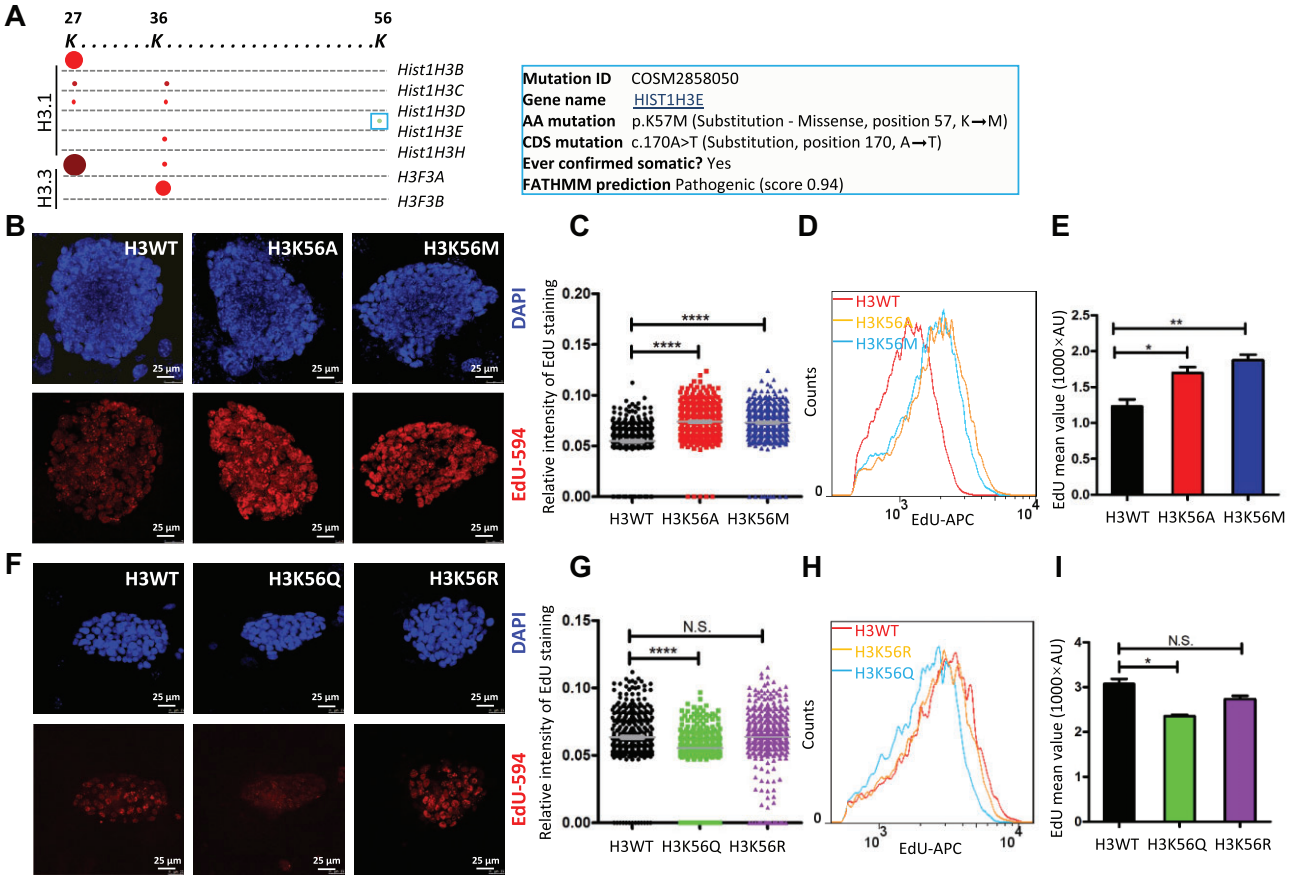

Figure 1 Effects of histone H3K56 mutants on replication. (**A**) Histone H3 site-specific K>M mutation scan in the COSMIC database. Three lysine sites on histone H3, namely K27, K36, and K56, which were substituted with methionine, are plotted. The diameter and color density of the circles indicate the frequency in the database. The annotation of H3K56M is listed on the right. (**B**) Immunofluorescence staining of EdU incorporation in mESCs carrying H3WT, H3K56A, and H3K56M. Cells were incubated with 10 μM EdU for 15 min. Fluo-594 was added by the Click-iT reaction, and photographs of the clone were obtained with confocal imaging. Scar bar, 25 μm. (**C**) Statistical results of relative intensity of EdU in each cell from immunofluorescence staining of H3WT, H3K56A, and H3K56M, as shown in **B**. (**D**) The mean EdU intensity in H3WT, H3K56A, and H3K56M detected by flow cytometry. The horizontal axis indicates the EdU level based on annexin V–allophycocyanin (APC) fluorescence, and the vertical axis presents cell counts. Different treatments are shown in different colors as indicated. (**E**) Statistical quantification of the mean EdU level in H3WT, H3K56A, and H3K56M by flow cytometry analysis, as shown in **D**. The bar graph shows the mean EdU incorporation in S phase. (**F** and **G**) Immunofluorescence staining (**F**) and statistical analysis (**G**) of EdU incorporation in mESCs carrying H3WT, H3K56Q, and H3K56R. The staining and quantification procedure was identical to that in **B** and **C**. Scar bar, 25 μm. (**H** and **I**) The mean EdU level in H3WT, H3K56Q, and H3K56R was determined by flow cytometry (**H**) and statistically quantified (**I**). Data from three independent experiments are presented as mean ± SEM. *$P < 0.05$, **$P < 0.01$, and ****$P < 0.0001$ (two-tailed *t*-test, $n = 3$). N.S. indicates not significant.

these data showed that enhanced S-phase EdU incorporation in H3K56M or H3K56A cells may be derived from the promotion of replication efficiency.

H3K56M and H3K56A mutant incorporation induces enhanced replication in mESCs

In order to explore the underlying mechanism behind replication promotion, we performed DNA fiber combing assays to detect the replication moving characters along genome. We labelled the replicating DNA for two rounds with a dUTP analog, first with 25 μM CldU for 10 min and then with 250 μM IdU for 20 min. After labelling, the genome DNA from cells was extensively fixed on slides, and then the replicating sites were stained with specific antibodies against CldU and IdU (Supplementary Figure S4). Data for the length of the second labelling of IdU without signal cease were collected and calculated (Figure 2A and B). The data showed that IdU signal extension per 20 min was obviously increased in both H3K56M and H3K56A, but decreased in H3K56Q, and not obviously changed in H3K56R compared with H3WT, which suggested that H3K56M and H3K56A promoted the replication speed.

mESCs can inherently trigger the replication machinery to protect against stress (Ge et al., 2015). To investigate how the enhanced replication responds to stress, we tested the

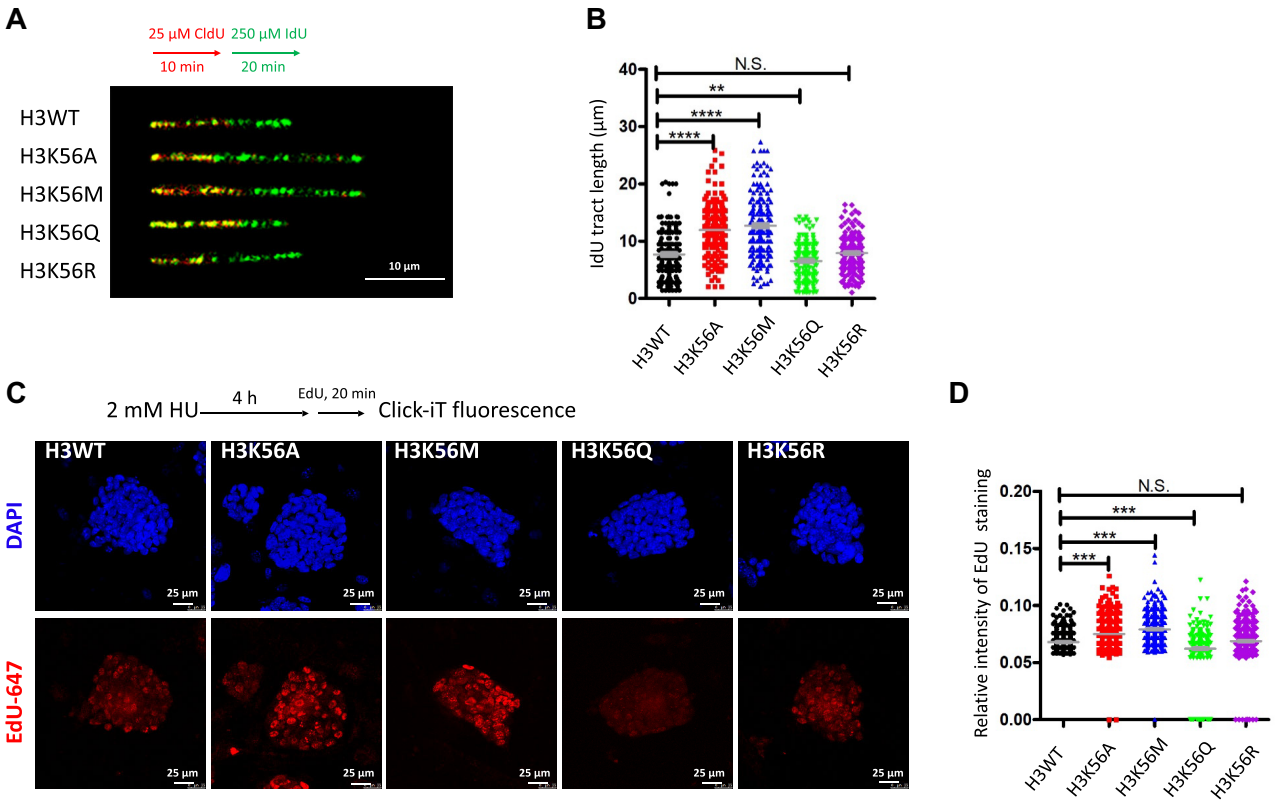

Figure 2 Effects of histone H3K56 mutants on DNA replication efficiency. (**A**) DNA fiber combing assays show replication fork speed in H3K56 mutants. Cells were labelled for 10 min with 25 μM CldU and were further incubated for 20 min with 250 μM IdU. Confocal images of DNA fiber analysis are shown. Red: CldU; green: IdU. Scar bar, 10 μm. (**B**) Statistical quantification of the IdU tract length in H3K56 mutants, as shown in **A**, with the median values marked on the graph. At least 100 replication tracts were quantified for each sample. (**C**) Immunofluorescence images of EdU staining in H3K56 mutants. Cells were incubated with 4 mM HU before EdU pulse. Fluo-647 was added by the EdU Click-iT reaction, and confocal images of mESCs carrying H3K56 mutants are shown. Scar bar, 25 μm. (**D**) Statistical quantification of EdU incorporation in the remaining replicative cells after HU blockade. Data from three independent experiments are presented as mean ± SEM. $^{**}P < 0.01$, $^{***}P < 0.001$, $^{****}P < 0.0001$ (two-tailed *t*-test, $n = 3$). N.S. indicates not significant.

recovery of EdU incorporation after release from hydroxyurea (HU)-induced replication blocking. Here, we detected the refiring EdU value after HU blocking in H3K56 mutants with confocal imaging analysis by scanning the whole clones by Z-axis projection and then quantified the positive EdU signal in each cell (Figure 2C and D; Supplementary Figure S5). The data showed that the capability of refiring EdU incorporation was obviously increased in both H3K56M and H3K56A mutants, but decreased in H3K56Q, and at a similar level in H3K56R compared with that in H3WT (Figure 2C and D). Taken together, our results demonstrated that H3K56M and H3K56A incorporation could promote replication.

H3K56M and H3K56A mutants mediate enhanced binding with Chk1 and MCM3 in mESCs

To study the mechanism of H3K56A/M in replication promotion, we attempted to identify its specific binding partners. We used the cell line carrying the H3K56A mutant fused with EGFP as described above and extracted the nuclear extract. Then, we captured the H3K56A complex by GFP trapping, and the candidates were identified by matrix-assisted laser desorption ionization-time of flight (MALDI-TOF) mass spectrometry (MS) (Figure 3A). Although a bulk of replication factors, such as MCM2–MCM7, were commonly detected in both histone H3WT- and H3K56A-binding proteins, the checkpoint protein Chk1 was specifically detected in H3K56A rather than H3WT and the top-score candidates of H3K56A-binding proteins are listed in Supplementary Table S1. We further confirmed the enhanced binding affinity between H3K56A and Chk1 protein, which clearly showed that Chk1 could be recruited to the deposited H3K56A but not H3WT, H3K9A, H3K27A, or H3K36A (Supplementary Figure S6). We then compared the enrichment level of Chk1 docked on the H3K56A mutant by GFP trapping and western blotting, and the data showed that H3K56A could recruit more Chk1 than other site-specific K>A mutants, such as H3K9A and H3K36A (Figure 3B). Furthermore, compared with H3WT, H3K9M, and H3K36M, both H3K56A and H3K56M exhibited the same enhanced binding affinity with MCM3 (Figure 3C),

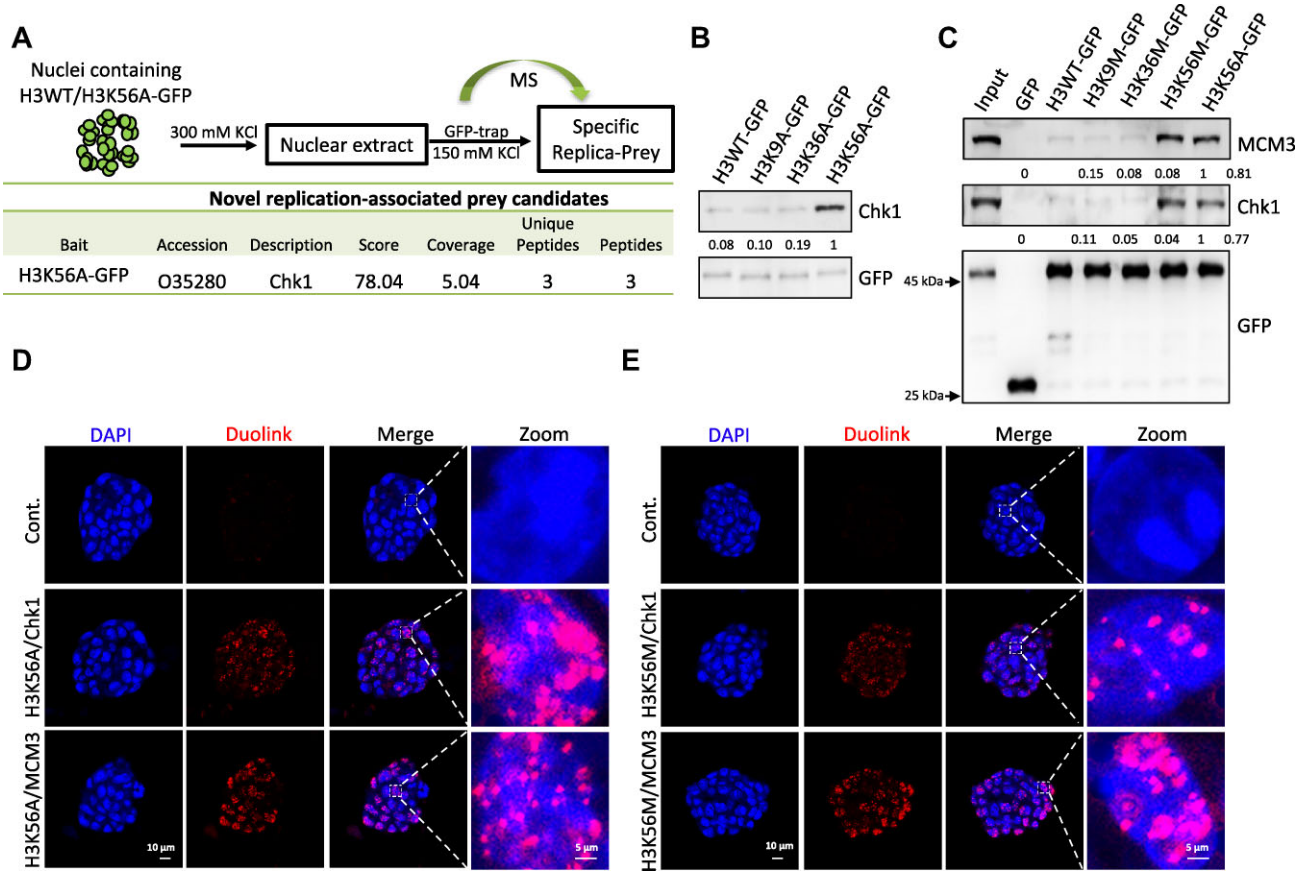

Figure 3 Histone H3K56M and H3K56A mutations enhance the affinity of binding with Chk1 and MCM3. (**A**) Detection of binding partners of H3K56A and identification of unique replication-associated candidates from H3K56A-immunoprecipitated products by MALDI-TOF. (**B**) Comparison of the Chk1-binding affinity of K>A mutants (H3K9A, H3K36A, and H3K56A) by GFP-trap immunoprecipitation and immunoblotting. H3WT was used as trap control. (**C**) Comparison of Chk1 and MCM3 binding with H3K9M, H3K36M, H3K56M, and H3K56A by GFP-trap immunoprecipitation and western blotting. H3WT was used as trap control and GFP was used as empty vector control. (**D** and **E**) Duolink PLA using antibodies against HA (rabbit) and Chk1 (mouse) or HA (mouse) and MCM3 (rabbit) was performed in H3K56A (**D**) and H3K56M (**E**) cells. Red spots represent protein–protein interaction couples. The control shown indicates the omission of the primary antibody against HA. Scar bar, 10 μm (original) and 5 μm (enlarged).

another replication factor interacting with Chk1 (Han et al., 2015). We further adopted Duolink proximity ligation assay (PLA) to detect the interaction between histone H3K56A or H3K56M with Chk1 and MCM3 in H3K56A and H3K56M mESCs. The data showed that MCM3 and Chk1, respectively, did interact with H3K56A or H3K56M *in vivo* (Figure 3D and E) and that MCM3 and Chk1 also had protein–protein interaction (Supplementary Figure S7). All these data showed that H3K56A/M mutants enhanced the ability to recruit Chk1 and MCM3 onto chromatin.

H3K56M and H3K56A protect MCM3 from degradation even in the absence of Chk1

Since replication promotion has been observed in H3K56M and H3K56A cell strains, more MCM3–Chk1 could also be recruited to facilitate stabilization of the replication fork (Lopes et al., 2001). We then asked how Chk1 affected MCM3 and the ORC in the mESC context. We first tested the effects of Chk1 knockdown on S-phase replication progression by an EdU incorporation assay and on protein levels of replisome candidates, including MCM and the ORC, by western blotting (Figure 4A and B). The data showed that the intensity of S-phase EdU incorporation in Chk1 knockdown cells was lower than that in the control (Figure 4A), and the levels of all the tested candidates, including MCM2, MCM3, ORC1, ORC6, and PCNA, in Chk1 knockdown cells strikingly declined compared with those in negative control cells (Figure 4B). We next analyzed changes in replisome machinery-related factors under Chk1-depleted conditions in H3K56A and H3K56M cell lines, and there were no obvious changes in these replisome candidates upon Chk1 depletion, indicating that H3K56A/M mutants could block Chk1 deficiency-induced replisome machinery instability (Figure 4C and D). However, H3WT cannot perform this function (Figure 4C and D). Therefore, we concluded that H3K56A/M mutants could protect the replisome machinery from dysfunctional interference even in the absence of Chk1.

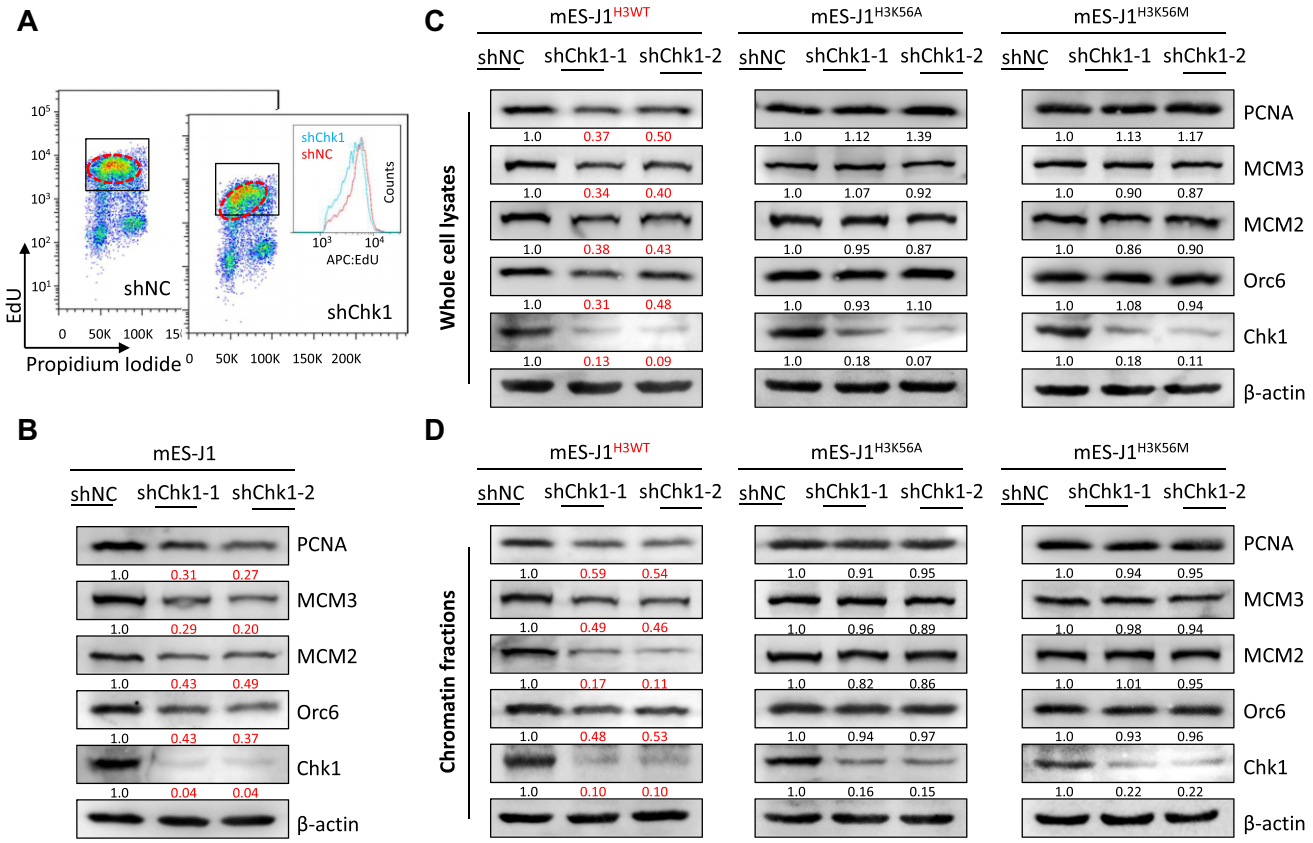

Figure 4 H3K56M and H3K56A protect MCM3 and replisome candidates from degradation even in the absence of Chk1. (**A**) Representative FACS images of EdU staining of mESCs transfected with shChk1 and shNC. The boxes show the cells in S phase, and the red dashed circles indicate the position of replicating cells. The intensity of APC fluorescence with arbitrary units in each labelled cell was analyzed and is represented in the inset. The horizontal axis shows the APC value of individual EdU-positive cells, and the vertical axis shows the number of detected cells. (**B**–**D**) Immunoblotting of the candidate MCM/ORC complexes in empty (**B**) or H3WT, H3K56A, and H3K56M (**C** and **D**) mESCs transfected with shNC and shChk1. Whole-cell lysates (**B** and **C**) or intact chromatin fractions (**D**) were used for analysis, and the signal intensities were calculated by Image J. The red numbers indicate significant changes.

H3K56M and H3K56A incorporation induces copy number amplification and interferes with local H3K56ac in mESCs

It is well known that overreplication can easily lead to DNA copy number variations (CNVs) (Arlt et al., 2012; Black et al., 2013). To study the physiological outcome of H3K56A/M mutants in mESCs, we performed a comparative genomic hybridization (CGH) array to detect CNVs in H3K56A and H3K56M mutant strains. The data showed that both mutant strains exhibited a high frequency of CNVs compared with the empty mESC strain, and all these CNVs displayed copy gains (Figure 5A). In these copy-gain regions, there were two common CNVs, namely qD1 and qD2.2, on Chr. 4 in both H3K56A and H3K56M strains. The qD1 region is reported as a region vulnerable to copy gain and exposed to highly frequent CNVs in nearly all of the mouse strains, but the qD2.2 region includes an important gene called *Mycl1* (Figure 5A and B), which is an oncogenic allele in humans and comprehensively expressed in multiple types of clinical cancers, such as lung, ovarian, and gastric cancers (Nau et al., 1985; Tsujino et al., 1990; Wu et al., 2003; Locke et al., 2015). Then, we verified copy gain in these two common regions as well as another region, called qA3, on Chr. 7 by quantitative polymerase chain reaction (qPCR). All the genome-gain regions exhibited a general increasing tendency in H3K56A and H3K56M compared with H3WT (Figure 5C and D; Supplementary Table S2). Additionally, the data showed that the mean reads per kilobase of transcript per million mapped reads value of typical genes located in the qD2.2 region was higher in H3K56A than in H3WT (Supplementary Figure S8A and B), which is identical to the outcome of CNVs.

H3K56ac is known as a favorable epigenetic modification in transcription activation, and incorporation of H3K56A/M mutations theoretically generates the dominant sequestration and thus reduces the occupancy of H3K56ac in the genome. To study the interplay between H3K56A/M mutants and H3K56ac modification in copy-gain regions, we analyzed the enrichment of H3K56ac and H3K56 mutants in the copy-gain regions by chromatin immunoprecipitation (ChIP)–qPCR. H3K56ac levels in all the tested copy-gain regions decreased in H3K56A and H3K56M strains compared with H3WT (Figure 5E). However, the distribution of ectopic H3K56A and H3K56M mutants showed

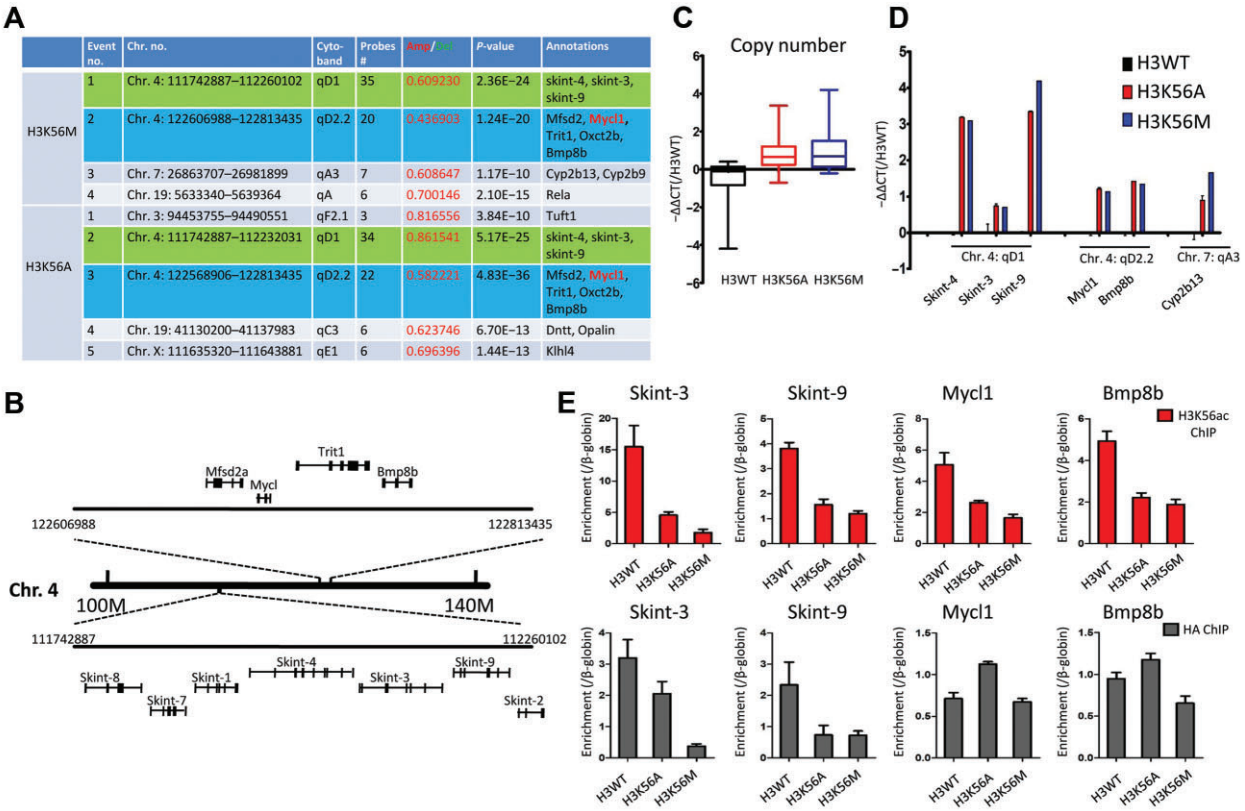

	Event no.	Chr. no.	Cyto-band	Probes #	Amp/Del	*P*-value	Annotations
H3K56M	1	Chr. 4: 111742887–112260102	qD1	35	0.609230	2.36E–24	skint-4, skint-3, skint-9
	2	Chr. 4: 122606988–122813435	qD2.2	20	0.436903	1.24E–20	Mfsd2, Mycl1, Trit1, Oxct2b, Bmp8b
	3	Chr. 7: 26863707–26981899	qA3	7	0.608647	1.17E–10	Cyp2b13, Cyp2b9
	4	Chr. 19: 5633340–5639364	qA	6	0.700146	2.10E–15	Rela
H3K56A	1	Chr. 3: 94453755–94490551	qF2.1	3	0.816556	3.84E–10	Tuft1
	2	Chr. 4: 111742887–112232031	qD1	34	0.861541	5.17E–25	skint-4, skint-3, skint-9
	3	Chr. 4: 122568906–122813435	qD2.2	22	0.582221	4.83E–36	Mfsd2, Mycl1, Trit1, Oxct2b, Bmp8b
	4	Chr. 19: 41130200–41137983	qC3	6	0.623746	6.70E–13	Dntt, Opalin
	5	Chr. X: 111635320–111643881	qE1	6	0.696396	1.44E–13	Klhl4

Figure 5 H3K56M and H3K56A mutant incorporation induces genome instability and copy number amplification in mESCs. (**A**) Collection results of the CGH array from H3K56M and H3K56A. Green and blue lanes indicate common amplification regions in both H3K56A and H3K56M. Gray lanes indicate the specific amplification regions. (**B**) Diagram of common amplification regions in genomic DNA. (**C**) CNV of the whole genome tested by qPCR. H3WT was used for normalization, and β-globin was used as an internal control. (**D**) Copy number amplification of the genes in common amplification regions tested by qPCR. H3WT was used for normalization, and β-globin was used as an internal control. (**E**) ChIP–qPCR results of H3K56ac (upper) and histone mutant (bottom) distribution in common copy-gain regions. The ChIP signal of β-globin was used as an internal control.

inconsistent tendencies in H3K56A and H3K56M strains compared with that in H3WT (Figure 5E). Meanwhile, H3K56ac occupancy in non-amplified regions did not show obvious decrease in H3K56A/M (Supplementary Figure S9). These data suggested that histone mutant incorporation may be random and the induced decrease of H3K56ac is the main outcome, which is likely the major driver directing copy gain in H3K56A/M mutants. Furthermore, we blocked the lysine acetylation transferase CBP/p300 activity by adding the specific inhibitor C646 to cells to detect the affinity change between the replisome complex and histone H3 when H3K56ac decreases, and the results indicated that the binding intensity of MCM3 and Chk1 on deposited H3 increased after inhibiting CBP/p300 activity compared with vehicle treatment (Supplementary Figure S10). This is additional evidence verifying the protective effects of H3K56ac on fine replication regulation.

H3K56M and H3K56A incorporation induces transcriptional adaptation of the oncogenetic signaling pathway in mESCs

Since genetic loci including *Mycl1*, a member of the *MYC* family, are amplified in H3K56M and H3K56A cells, and the *MYC* family amplification is a frequent genetic variation in cancer and plays a vital role in carcinoma development, we performed RNA sequencing (RNA-seq) analysis to investigate changes in transcriptional profiles of ESCs expressing H3K56A. The data showed that H3K56A cells exhibited weak transcriptome remodeling, and just a limited number of genes showed obvious differential expression (109 upregulated and 112 downregulated) compared with the expression in H3WT cells (Supplementary Figure S8 and Table S3). To better study the mechanism of transcriptome regulation, we performed Gene Ontology (GO) pathway analysis based on the upregulated and downregulated groups of genes (Figure 6A). The results showed that the upregulated genes were involved in GO terms of the mitogen-activated protein kinase (MAPK) and JUN kinase pathways, and the downregulated genes were involved in the intrinsic apoptotic signaling pathway (Figure 6A and B; Supplementary Table S2). Therefore, in addition to replication-derived genetic alteration, the outcomes of transcriptome remodeling, including both the upregulated genes in the MAPK–JUN kinase pathway and the downregulated genes in apoptotic signal pathway activity, supply additional stimuli to reinforce the capability of

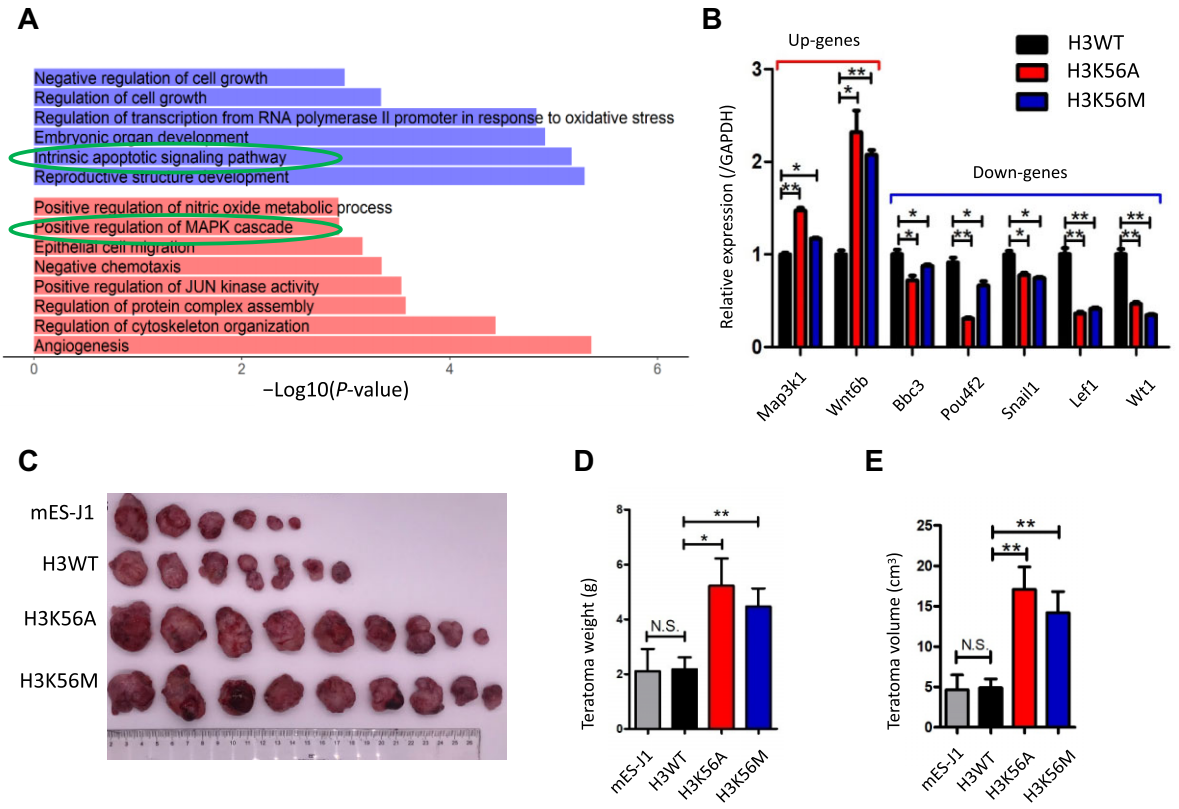

Figure 6 H3K56M and H3K56A mutant incorporation induces transcriptional adaptation and triggers carcinoma formation. (**A**) GO term analysis of differentially expressed genes in mESCs carrying H3K56A compared with H3WT. The upregulated genes are labelled in red, and the downregulated genes are labelled in blue. (**B**) qPCR confirmation of the typical apoptotic genes and MAPK–JUN kinase pathway genes marked with green circles in **A**. Data from three independent experiments are presented as mean ± SEM. $*P < 0.05$, $**P < 0.01$ (two-tailed *t*-test, $n = 3$). (**C**–**E**) Carcinoma formation of mESC strains (empty, H3WT, H3K56A, and H3K56M) in nude mice. Teratomas were collected (**C**) and the weight (**D**) and volume (**E**) were quantified 4 weeks after injection of mESC strains. Error bars indicate SD ($n = 10$ mice in each group), and *P*-values were calculated with *t*-tests. $*P < 0.05$, $**P < 0.01$. N.S. indicates no significance.

cancerous proliferation. Therefore, we next explored the ability of carcinoma formation in nude mice by subcutaneous injection, and the data showed that both H3K56M and H3K56A cells acquired an enhanced ability to form xenograft carcinomas, i.e. the weight and volume of the carcinoma produced from H3K56M and H3K56A cells obviously exceeded those from H3WT cells and empty mESCs (Figure 6C–E). These results clarified the links between H3K56A/M-induced physiological outcomes and the underlying mechanism.

Discussion

Substitution of conserved histone sites usually occurs on certain alleles of histone H3 gene clusters and is correlated with tumor development (Funato and Tabar, 2018). Here, we studied the functional behavior of mESCs with ectopic expression of H3K56M, a sense mutation on *HIST1H3E* searched from the cancer database (Figure 1A), and a series of other H3K56 mutants. H3K56 single-site mutation did not impair its own ability to deposit on chromatin, as analysis of the whole nuclear proteins, GFP-trap analysis of the chromatin complex, and cross-linked chIP clearly detected tail-tagged mutants by western blotting (Figure 3; Supplementary Figures S1C, D and S6). Interestingly, different types of site mutations on H3K56 have different effects on replication. We first found that fine effects of H3K56A, H3K56M, H3K56Q, and H3K56R on DNA replication were distinct from each other. H3K56M and H3K56A incorporation could obviously promote replication efficiency, and recovery capability from the release of HU blockage in H3K56M and H3K56A was much higher than that in H3WT and other cells, which indicated that replication could be strikingly activated by H3K56M or H3K56A incorporation and could not be disrupted by acute stress (Figures 1 and 2). The major characteristic of H3K56M and H3K56A is their nonpolar side chain, so we hypothesized that depolarization of the side chain may be the determining factor interfering with the replication process. We found higher replication velocity in H3K56M and H3K56A cells, but the deep fine mechanism of replication dynamics still remains unclear. We are not sure whether the frequency of replication origin firing has changed, and thus further research is necessary. Furthermore, we found the ectopic expression levels of H3K56 mutants were

~5% of total H3 (Supplementary Figure S1D). Of all reported cases, only one-allele mutation was found in certain cases, such as *H3F3A*, *H3F3B*, and *HIST1H3E*, suggesting that a single site mutation in one allele is sufficient to produce clinical and epigenetic outcomes (Wu et al., 2012; Behjati et al., 2013; Wan et al., 2018). The 5% is a considerable level that is quite close to the proportion of the one-allele product to the overall H3 level. Thus, we readily found that incorporation of relatively low levels of H3K56 mutants perturbed the global replication efficiency, but this is another issue that requires careful consideration of dosage and multiallelic mutagenesis.

There is local crosstalk between H3K56ac and H3K56A/M, especially in copy-gain regions. Unlike the ability of cancer-related H3K36M and H3K27M to modify the epigenetic landscape, H3K56M and H3K56A induced a decrease in H3K56ac enrichment at copy-gain regions in our research (Figure 5), but global modification levels of H3K56ac and H3K56me1/3 did not show obvious changes (Supplementary Figure S11), indicating that H3K56M and H3K56A incorporation has a dominant-negative effect on local H3K56ac levels in amplified regions (Lewis et al., 2013; Yuen and Knoepfler, 2013; Fang et al., 2016; Lu et al., 2016). However, H3K56M and H3K56A did not have likely binding–killing interaction activity, as found in H3K27M or H3K36M (Fang et al., 2016; Lu et al., 2016; Mohammad et al., 2017; Piunti et al., 2017). Although Suv39h was reported as a candidate H3K56me3 methyltransferase, its methyltransferase activity could not be impaired by either H3K56A or H3K56M, as there was no obvious change in the level of H3K9me3, the major product of Suv39h (Supplementary Figure S11). In addition, remodeling of transcription could not provide evidence for the epigenetic mechanism of H3K56A on H3K56ac, and RNA-seq analysis showed that the number of downregulated genes was equal to that of upregulated genes in H3K56A cells, which indicated a limited potential ability for general transcriptional regulation induced by H3K56A incorporation (Supplementary Figure S8B). Thus, H3K56ac redistribution on the genome is probably the response to DNA replication stress in the copy-gain regions observed in mESCs carrying H3K56M and H3K56A mutants.

H3K56A/M mutants showed replication activation by enhancing MCM3 and Chk1 recruitment on chromatin through protein–protein interactions (Figure 3). Histone H3 with hypo-H3K56ac induced by p300 inhibition also produced the same enhancing effect (Supplementary Figure S10). Thus, it is suggested that H3K56 deacetylation may contribute to reinforcing the binding of replication factors on chromatin and triggering replication activation; however, histone mutants may function independently as novel proteins, and global deacetylation levels in response to p300 inhibition targeting a very large number of protein candidates make the fine regulation mechanism between replication and H3K56ac more complex. Therefore, we can only rationally conclude that the H3K56 site is important for replication activation on the chromatin platform, and either modification imbalance or site mutation at this vital site can perturb the mechanism of action of the replication machinery.

The MCM2–MCM7 complex directly participated in replication-coupling nucleosome dynamics through the activity of the H3–H4 tetramer-specific chaperone of MCM2 (Clement and Almouzni, 2015; Huang et al., 2015). The interplay of the Chk1–MCM3 axis is known to be a mechanism that maintains the fidelity of replication initiation and plays important roles in maintaining genome stability (Bailis et al., 2008; Han et al., 2015). Chk1 could prevent the start of error-prone DNA replication by delaying activation of the MCM2–MCM7/ORC complex until the error was repaired (Bailis et al., 2008; Han et al., 2015). We also detected Chk1-dependent phosphorylation of MCM3 in our test (Supplementary Figure S12), and thus Chk1 has kinase activity in this pathway in mESCs. Surprisingly, our research data showed that Chk1 is essential for maintaining the stability of the replisome candidate pool. Chk1 knockdown induced obvious degradation of the MCM2–MCM7/ORC complex and thus prohibited DNA replication, but replisome factors remained stable in H3K56A or H3K56M cells regardless of the presence or absence of Chk1 (Figure 4). Therefore, we concluded that Chk1 was located downstream of MCM3 recruitment in mESCs, and the enhanced binding of Chk1 to H3K56A or H3K56M was an intrinsic response to the high potential of extra replisome loading. This is also why the ability of carcinoma formation on H3K56A/M cells transfected with short hairpin interference RNAs (shRNAs) against Chk1 (shChk1) is much stronger than that on H3K56A/M cells alone (Supplementary Figure S13). Our research indicated that histone H3K56A and H3K56M supply an effective platform for Chk1 and MCM3 by protein–protein interaction, which not only triggered more efficient replication but also recruited more checkpoint activity to try to guarantee genome stability under highly active replication.

Another opinion is that replication-coupled H3K56ac in yeast is beneficial for prevention of DNA re-replication and thus maintains genome stability (Ide et al., 2013; Kadyrova et al., 2013). Otherwise, mESCs are a concrete type of cells characterized by tolerance of ultrafast proliferation under replication stress and easy escape from genomic instability (Ahuja et al., 2016). In combination with the function of H3K56M and H3K56A, we speculated that H3K56ac in ESCs might play a similar balancing role in maintaining replication and genome stability, and new replication factory activation in H3K56M and H3K56A cells undoubtedly reinforced the stress on this balance. The direct outcome of H3K56 mutations was a decrease in H3K56ac distribution in amplified genomic regions, which released local constraints on the replication machinery (Figures 4 and 5). Stem cell-like properties are one of the internal drivers of cancer metastasis and evolution (Rothenberg and Clarke, 2009). Our finding based on ESCs can be used to better understand the mechanism of cancer adaptation in H3K56 mutant incorporation and H3K56ac rearrangement.

Furthermore, we found that the physiological outcome of H3K56M or H3K56A mutation is more likely the favorable choice during cancer evolution. Copy number amplification was considered to be derived from the replication machinery hijacked by

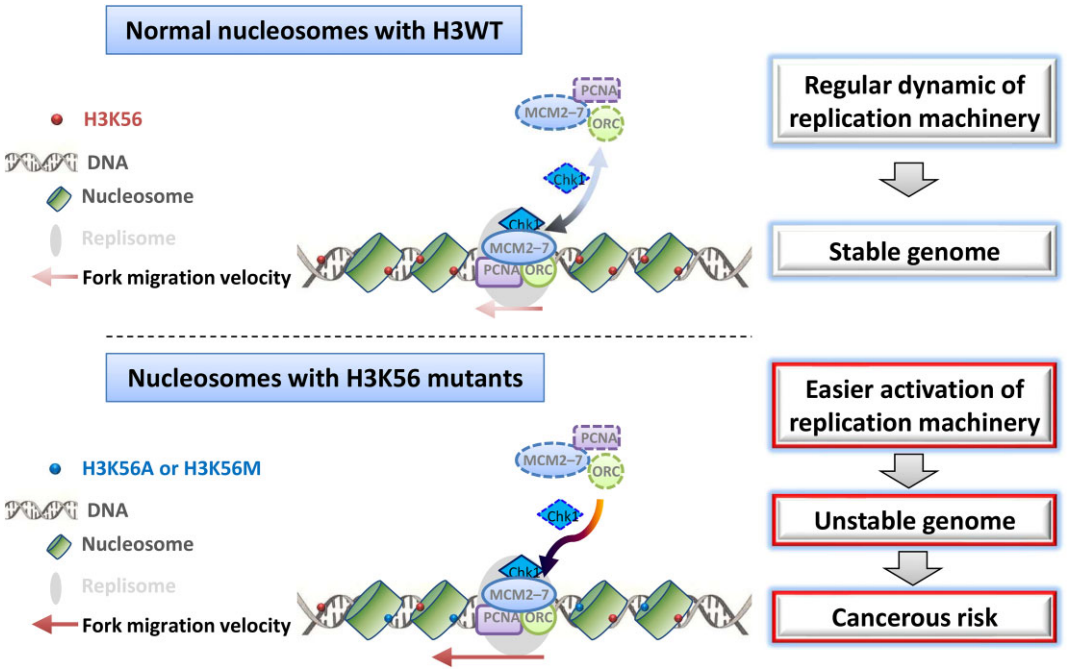

Figure 7 Diagram of biological functions of the essential histone H3K56 and the mechanism of action of H3K56 mutants in replication. In normal nucleosomes containing H3WT, the replication process is controlled under a regular schedule, and dynamic variation between replisome firing and candidate recruitment is coordinated and regulated by Chk1. However, nucleosomes containing histone H3K56A or H3K56M perturb this dynamic balance by triggering recruitment of replication candidates and thus cause more replication activation, which promotes genome instability and cancer risk.

H3K56M and H3K56A; it is surprising that amplification selectively occurred in the specific genomic loci of qD2.2 in the Chr. 4 region, which tethers the oncogene *Mycl1*. Amplification of the *MYC* gene family is a common marker in multiple clinical cases, including lung, ovarian, and gastric cancers. *Mycl1* copy gain is a frequent event in these cancers (Nau et al., 1985; Tsujino et al., 1990; Wu et al., 2003). Therefore, *Mycl1* copy gain may produce a genetic hallmark for cancer evolution and contribute to enhanced ability of carcinoma formation. It is found that high frequency of oncogenic copy variations is common in DIPG clinical cases with H3.3K27M (Paugh et al., 2010), but there were no CNV data contained in COSMIC cases with H3K56M; thus, whether *Mycl1* amplification is a concern in H3K56M clinical research needs more proofs.

Selective adaptation to the transcription of H3K56M and H3K56A is another interesting event. The upregulated genes were involved in the MAPK–JUN kinase pathway, and the downregulated genes were involved in apoptotic signaling pathways. Differential expression of both gene groups indicated a cancer promoting tendency (Figure 6A and B). In previous work, it was found that the H3K56ac level in cancer is responsive to MAPK signaling pathways, specifically to PI3K–AKT activation, and continuous Ras firing can induce an obvious decrease in H3K56ac (Liu et al., 2012). However, when we produced the same ectopically activated Ras in mESCs, there were no obvious changes in H3K56ac levels (Supplementary Figure S14). Therefore, H3K56A/M incorporation in ESCs may reconstruct the conserved interplay between H3K56ac modification and MAPK signaling pathways and switch their mediator from Ras to others, the fine mechanism of which needs further study. Downregulation of apoptosis-related genes reflects an inhibitory potential upon cell death, which is probably another sign of transcriptional adaptation contributing to cancer development. Therefore, although we cannot fully explain the transcription mechanism in detail, the general output of transcriptional remodeling induced by H3K56A or H3K56M incorporation is undoubtedly a second powerful promoter of cancer development.

In summary, we systematically studied the behavior of histone H3K56 mutants in mESCs and found that chromatin-deposited H3K56M and H3K56A could participate in replication machinery recruitment and generate a cascade-like effect on both replication and transcription regulation to adapt to enhanced proliferation (Figure 7). However, whether H3K56M or other H3K56 mutants actually play important roles in cancer remains an unanswered question; more screening and research efforts are needed in the future. Our study explains the importance of the H3K56 site in the harmonization of replication with physiological acquisition, which raises the possibility that the site specificity of H3K56 can be considered an anticancer drug target, acting by correctly regulating replication machinery usage under replicative stress.

Materials and methods

Plasmid construction, transfection, and virus production

Coding sequences of histone H3.1 were cloned from a human cDNA library and used for point mutagenesis to produce K56M/A/Q/R. Then, the resulting mutant sequences were tagged with the HA-coding sequence at the 3′-terminus and cloned into pEF-CSII-IRES-EGFP. These plasmids were used for lentivirus particle production. The H3 and mutant sequences were cloned into the pCAG-EGFP-N1 vector, and fusion proteins tagged with EGFP at their C-termini were obtained. These plasmids were used for transient expression.

shChk1 and negative control shRNA (shNC) were synthesized and ligated into GV-298 (Genechem) driven by the U6 promoter. mCherry was used as the positive clone-sorting reporter. Sequences of shChk1 are as follows. shChk1-1: CCGGGCC ACGAGAATGTAGTGAAATCTCGAGATTTCACTACATTCTCGTGGCTTTTT; shChk1-2: CCGGGCAACGGTATTTCGGCATAATCTCGAGATTATGCC GAAATACCGTTGCTTTTT.

Cell culture, primary cells, and generation of stable cell lines

mESCs (J1 strain) were cultured and used to express different histone mutants and target proteins by plasmid transfection as detailed in Supplementary Materials and methods.

Cell staining and EdU cell proliferation detection

DNA replication was tested using a Click-iT EdU Staining Kit (Thermo Fisher Scientific, C10634, C10640). EdU staining assay was performed as described in Supplementary Materials and methods. mESC pluripotency was roughly evaluated by quantifying the *para*-nitrophenol product formation catalyzed by alkaline phosphatase (SIDANSAI, Shanghai, China, #1101-050).

Antibodies and other reagents

All antibodies and other reagents used in this study are listed in Supplementary Materials and methods.

DNA fiber assay

DNA combing analysis was performed as described (Bianco et al., 2012) and also detailed in Supplementary Materials and methods.

Duolink PLA

The Duolink® PLA was performed using the Duolink In Situ Orange Starter Kit (Merck, DUO92101). Detailed protocols are described in Supplementary Materials and methods.

Ethics statement and teratoma experiments

All animal studies were approved by the Animal Care Committee of Tongji University School of Medicine. Three-week-old nude mice were used for cell transplantation. Single-cell suspensions of transgenic mESCs were counted, and the cell concentration was adjusted to 10^6/ml in Dulbecco's modified Eagle's medium containing 10% Matrigel (Corning, #354230). Then, cells were injected subcutaneously into nude mice (0.1 ml per mouse). Tumor size was measured every week. After 4 weeks, the teratoma tissues were dissected and weighed.

Nucleic acid purification and copy number assay

mESCs of 6-week-old transgenic mice were collected, and genomic DNA was purified using the TIANamp Genomic DNA Kit (Tiangen, DP304). Total RNA was extracted from cells using the RNAiso Plus reagent (TaKaRa, #9109).

Genomic DNA from H3WT, H3K56M, and H3K56A was used for exome sequencing. For CGH to assay CNV, genomic DNA from empty mESCs under the same passage conditions was used as the reference DNA of mutants. Array-based CGH analysis was performed using the Agilent Mouse Genome Microarray Kit 4 × 180K (Agilent Technologies).

RNA-seq and bioinformatics analysis

RNA-seq libraries were prepared with the TruSeq RNA Library Prep Kit v2 (Illumina) according to the manufacturer's instructions and sequenced on an Illumina HiSeq X-10 or HiSeq 2000 instrument by Novogene.

Gene expression profiles were analyzed by Cuffdiff2 (v2.2.1), and the filtration criteria were set as fold change >1.5 and q-value <0.05. The Gene Ontology Consortium database (http://www.geneontology.org/) was used to identify the enriched biological processes.

ChIP and qPCR

ChIP assays were performed according to the procedure of the Faham laboratory. The details can be downloaded from http://farnham.genomecenter.ucdavis.edu/pdf/FarnhamLab ChIP%20Protocol.pdf.

The ChIP DNAs were measured with the Qubit 2.0 fluorometer dsDNA HS Assay (Thermo Fisher Scientific) and used as qPCR templates. Primers for the copy-gain region were used for SYBR Green I detection qPCR, and the β-globin region was used as an internal normalization control.

Co-IP for histone mutants

Vectors of histone H3 mutants fused with EGFP were transiently transfected into mESCs using XfectTM mESC Transfection Reagent (TaKaRa, #631320). Nuclear extraction from cells, co-IP assays, and western blotting analysis were performed as described in Supplementary Materials and methods.

Interaction between histone H3 and replication-associated proteins

mESCs carrying H3WT-GFP or H3K56-GFP were collected to prepare whole nuclear extracts using Benzonase (Merck, E1014) capture buffer as described in Supplementary Materials and methods. The H3-GFP proteins captured by GFP-trap agarose and MCM3 and Chk1 from the resulting products were quantitatively assayed by western blotting, and GFP was used as an internal loading control.

Statistical analysis

Unless otherwise noted, all data were from three independent experiments and were presented as mean ± SEM. Unpaired two-tailed Student's *t*-test was used to compare two groups, with significant differences being considered as $*P < 0.05$, $**P < 0.01$, $***P < 0.001$, and $****P < 0.0001$.

Supplementary material

Supplementary material is available at *Journal of Molecular Cell Biology* online.

Acknowledgements

We thank Prof. Fang-Lin Sun (Research Center for Translational Medicine, East Hospital, School of Life Sciences and Technology, Tongji University) for comments on the manuscript and helpful discussion.

Funding

This work was supported by grants from the National Key Research and Development Program of China (2017YFA0103301), the National Natural Science Foundation of China (81972743), and China Postdoctoral Science Foundation (2020M671205).

Conflict of interest: none declared.

Author contributions: X.K.: conception and design, collection and assembly of data, data analysis and interpretation, and manuscript writing. X.Y: data analysis and interpretation. X.G., Y.L., and C.Y.: collection and assembly of data. H.W.: conception and design, administrative support, data analysis and interpretation, and final approval of manuscript. J.C.: conception and design, financial support, administrative support, manuscript writing and revision, and final approval of manuscript.

References

Ahuja, A.K., Jodkowska, K., Teloni, F., et al. (2016). A short G1 phase imposes constitutive replication stress and fork remodelling in mouse embryonic stem cells. Nat. Commun. *7*, 10660.

Arlt, M.F., Wilson, T.E., and Glover, T.W. (2012). Replication stress and mechanisms of CNV formation. Curr. Opin. Genet. Dev. *22*, 204–210.

Bailis, J.M., Luche, D.D., Hunter, T., et al. (2008). Minichromosome maintenance proteins interact with checkpoint and recombination proteins to promote S-phase genome stability. Mol. Cell. Biol. *28*, 1724–1738.

Behjati, S., Tarpey, P.S., Presneau, N., et al. (2013). Distinct H3F3A and H3F3B driver mutations define chondroblastoma and giant cell tumor of bone. Nat. Genet. *45*, 1479–1482.

Bianco, J.N., Poli, J., Saksouk, J., et al. (2012). Analysis of DNA replication profiles in budding yeast and mammalian cells using DNA combing. Methods *57*, 149–157.

Black, J.C., Manning, A.L., Van Rechem, C., et al. (2013). KDM4A lysine demethylase induces site-specific copy gain and rereplication of regions amplified in tumors. Cell *154*, 541–555.

Che, J., Smith, S., Kim, Y.J., et al. (2015). Hyper-acetylation of histone H3K56 limits break-induced replication by inhibiting extensive repair synthesis. PLoS Genet. *11*, e1004990.

Chen, C.C., Carson, J.J., Feser, J., et al. (2008). Acetylated lysine 56 on histone H3 drives chromatin assembly after repair and signals for the completion of repair. Cell *134*, 231–243.

Clement, C., and Almouzni, G. (2015). MCM2 binding to histones H3–H4 and ASF1 supports a tetramer-to-dimer model for histone inheritance at the replication fork. Nat. Struct. Mol. Biol. *22*, 587–589.

Corpet, A., and Almouzni, G. (2009). A histone code for the DNA damage response in mammalian cells? EMBO J. *28*, 1828–1830.

Dai, J., Hyland, E.M., Yuan, D.S., et al. (2008). Probing nucleosome function: a highly versatile library of synthetic histone H3 and H4 mutants. Cell *134*, 1066–1078.

Das, C., Lucia, M.S., Hansen, K.C., et al. (2009). CBP/p300-mediated acetylation of histone H3 on lysine 56. Nature *459*, 113–117.

Fang, D., Gan, H., Lee, J.H., et al. (2016). The histone H3.3K36M mutation reprograms the epigenome of chondroblastomas. Science *352*, 1344–1348.

Funato, K., and Tabar, V. (2018). Histone mutations in cancer. Annu. Rev. Cancer Biol. *2*, 337–351.

Ge, X.Q., Han, J., Cheng, E.C., et al. (2015). Embryonic stem cells license a high level of dormant origins to protect the genome against replication stress. Stem Cell Rep. *5*, 185–194.

Han, J., Zhou, H., Horazdovsky, B., et al. (2007). Rtt109 acetylates histone H3 lysine 56 and functions in DNA replication. Science *315*, 653–655.

Han, X., Mayca Pozo, F., Wisotsky, J.N., et al. (2015). Phosphorylation of minichromosome maintenance 3 (MCM3) by checkpoint kinase 1 (Chk1) negatively regulates DNA replication and checkpoint activation. J. Biol. Chem. *290*, 12370–12378.

Huang, H., Stromme, C.B., Saredi, G., et al. (2015). A unique binding mode enables MCM2 to chaperone histones H3-H4 at replication forks. Nat. Struct. Mol. Biol. *22*, 618–626.

Ide, S., Saka, K., and Kobayashi, T. (2013). Rtt109 prevents hyper-amplification of ribosomal RNA genes through histone modification in budding yeast. PLos Genet. *9*, e1003410.

Kadyrova, L.Y., Mertz, T.M., Zhang, Y., et al. (2013). A reversible histone H3 acetylation cooperates with mismatch repair and replicative polymerases in maintaining genome stability. PLos Genet. *9*, e1003899.

Lewis, P.W., Muller, M.M., Koletsky, M.S., et al. (2013). Inhibition of PRC2 activity by a gain-of-function H3 mutation found in pediatric glioblastoma. Science *340*, 857–861.

Li, Q., Zhou, H., Wurtele, H., et al. (2008). Acetylation of histone H3 lysine 56 regulates replication-coupled nucleosome assembly. Cell *134*, 244–255.

Liu, Y., Wang, D.L., Chen, S., et al. (2012). Oncogene Ras/phosphatidylinositol 3-kinase signaling targets histone H3 acetylation at lysine 56. J. Biol. Chem. *287*, 41469–41480.

Locke, M.E., Milojevic, M., Eitutis, S.T., et al. (2015). Genomic copy number variation in Mus musculus. BMC Genomics *16*, 497.

Lopes, M., Cotta-Ramusino, C., Pellicioli, A., et al. (2001). The DNA replication checkpoint response stabilizes stalled replication forks. Nature *412*, 557–561.

Lu, C., Jain, S.U., Hoelper, D., et al. (2016). Histone H3K36 mutations promote sarcomagenesis through altered histone methylation landscape. Science *352*, 844–849.

Masumoto, H., Hawke, D., Kobayashi, R., et al. (2005). A role for cell-cycle-regulated histone H3 lysine 56 acetylation in the DNA damage response. Nature *436*, 294–298.

Mohammad, F., Weissmann, S., Leblanc, B., et al. (2017). EZH2 is a potential therapeutic target for H3K27M-mutant pediatric gliomas. Nat. Med. *23*, 483–492.

Nau, M.M., Brooks, B.J., Battey, J., et al. (1985). L-myc, a new myc-related gene amplified and expressed in human small cell lung cancer. Nature *318*, 69–73.

Pal, S., Graves, H., Ohsawa, R., et al. (2016). The commercial antibodies widely used to measure H3 K56 acetylation are non-specific in human and Drosophila cells. PLoS One *11*, e0155409.

Paugh, B.S., Qu, C., Jones, C., et al. (2010). Integrated molecular genetic profiling of pediatric high-grade gliomas reveals key differences with the adult disease. J. Clin. Oncol. *28*, 3061–3068.

Piunti, A., Hashizume, R., Morgan, M.A., et al. (2017). Therapeutic targeting of polycomb and BET bromodomain proteins in diffuse intrinsic pontine gliomas. Nat. Med. *23*, 493–500.

Recht, J., Tsubota, T., Tanny, J.C., et al. (2006). Histone chaperone Asf1 is required for histone H3 lysine 56 acetylation, a modification associated with S phase in mitosis and meiosis. Proc. Natl Acad. Sci. USA *103*, 6988–6993.

Rothenberg, M., and Clarke, M.F. (2009). Chapter 53—cancer stem cells. In: Lanza, R., Gearhart, J. Hogan, B., et al. (eds). Essentials of Stem Cell Biology (2nd edn). San Diego: Academic Press, 467–483.

Shan, C.M., Wang, J., Xu, K., et al. (2016). A histone H3K9M mutation traps histone methyltransferase Clr4 to prevent heterochromatin spreading. eLife *5*, e17903.

Tsujino, T., Yoshida, K., Nakayama, H., et al. (1990). Alterations of oncogenes in metastatic tumours of human gastric carcinomas. Br. J. Cancer *62*, 226–230.

Wan, Y.C.E., Liu, J., and Chan, K.M. (2018). Histone H3 mutations in cancer. Curr. Pharmacol. Rep. *4*, 292–300.

Williams, S.K., Truong, D., and Tyler, J.K. (2008). Acetylation in the globular core of histone H3 on lysine-56 promotes chromatin disassembly during transcriptional activation. Proc. Natl Acad. Sci. USA *105*, 9000–9005.

Wu, G., Broniscer, A., McEachron, T.A., et al. (2012). Somatic histone H3 alterations in pediatric diffuse intrinsic pontine gliomas and non-brainstem glioblastomas. Nat. Genet. *44*, 251–253.

Wu, R., Lin, L., Beer, D.G., et al. (2003). Amplification and overexpression of the L-MYC proto-oncogene in ovarian carcinomas. Am. J. Pathol. *162*, 1603–1610.

Xu, F., Zhang, K., and Grunstein, M. (2005). Acetylation in histone H3 globular domain regulates gene expression in yeast. Cell *121*, 375–385.

Yu, Y., Song, C., Zhang, Q., et al. (2012). Histone H3 lysine 56 methylation regulates DNA replication through its interaction with PCNA. Mol. Cell *46*, 7–17.

Yuen, B.T., and Knoepfler, P.S. (2013). Histone H3.3 mutations: a variant path to cancer. Cancer Cell *24*, 567–574.